Structural stability and half-metallicity of the zinc-blende phase of $Al_{1-x}Cr_xAs$: Density-functional study

Yong-Hong Zhao* and Guo-Ping Zhao
College of Physics and Electronic Engineering, Sichuan Normal University, Chengdu 610066, China

Yong Liu
College of Science, Yanshan University, Qinhuangdao 066004, People's Republic of China

Bang-Gui Liu
Institute of Physics, Chinese Academy of Sciences, Beijing 100190, China
and Beijing National Laboratory for Condensed Matter Physics, Beijing 100190, China

(Received 13 July 2009; revised manuscript received 25 October 2009; published 17 December 2009)

An accurate full-potential linear augmented plane waves method has been used to investigate the structural stability, half-metallic ferromagnetism of the zinc-blende phase of the ferromagnetic semiconductor alloy $Al_{1-x}Cr_xAs$. The relative stability of the zinc-blende phase with respect to the NiAs one and the ferromagnetism to the antiferromagnetism are confirmed by comparing total energy of various structures. Full optimization for all these structures is performed, including the cell volume, c/a for tetrahedral cells and internal parameters. Our calculation shows that when the Cr composition is less than 30%, the zinc-blende phase is more stable, whereas the NiAs one is more stable for more Cr composition. Therefore, bulk $Al_{1-x}Cr_xAs$ with zinc-blende structure can be obtained when x is smaller than 0.3, whereas only epitaxial films can exist for larger x. For all these compounds with x ranging from 0.125 to 1.0, robust half-metallic ferromagnetism is found in the zinc-blende phase. In addition, the effects of the spin-orbital interaction are considered and the total magnetic moments including both the spin and orbital contributions are presented. The spin-orbital interaction will destroy the perfect half-metallic ferromagnetism by reflecting some majority-spin states into the minority-spin gap, however, the decrease of the spin-polarization is only about 0.2% for all substitutional cases. At last, we give the exchange parameters and consecutively the Curie temperature within the mean-field approximation. Our systematical calculation for $Al_{1-x}Cr_xAs$ is useful to elucidate the half-metallic ferromagnetism in $Al_{1-x}Cr_xAs$ and to explore high-performance spintronic devices based on $Al_{1-x}Cr_xAs$ in future information technologies.

DOI: 10.1103/PhysRevB.80.224417 PACS number(s): 75.90.+w, 71.20.−b, 75.50.−y, 75.75.+a

I. INTRODUCTION

Spintronic devices, which exploit both the spin and charge of electrons, are the most promising candidates for future applications in information technologies.[1] Highly spin-polarized ferromagnets, especially half-metallic ferromagnets (HMFs) are key ingredients for the future high-performance spintronic devices. Since the discovery of de Groot *et al.* in 1983,[2] HMFs have attracted much attention due to their perfect spin polarization near the Fermi level.[3] Although there are many kinds of HMFs, such as Heusler alloys,[4] some transition-metal (TM) oxides[5,6] and diluted magnetic semiconductors (DMSs),[7] only those with higher (usually above the room temperature) Curie temperature and good compatibility in structure and conductivity with traditional semiconductors can be used in future spintronic devices.[8,9] One popular way approaching to HMFs is partly substituting main group metals for TMs in traditional II-V, II-VI, and IV-VI semiconductors,[7] especially those with large semiconducting gaps. Many useful DMSs or HMFs, based on GaAs,[10] GaN,[11] AlN,[12] GeTe,[13] etc., have been found experimentally and theoretically by this way.

AlAs is an important III-V semiconductor, which crystallizes into the zinc-blende (ZB) phase with a wide indirect energy gap of about 2.3 eV between the Γ point and the X one.[14–16] Although unstable in air, AlAs and related materials are important for high-speed resonant tunneling diodes.[9,17] Replacing all Al atoms in AlAs with Cr, ZB CrAs can be obtained, which has a ferromagnetic Curie temperature of about 400 K.[18] Although the ZB structure is (meta)stable for CrAs, it has been grown by the molecular-beam epitaxy method.[18–20] ZB CrAs has been regarded as an important spintronic material because of its high ferromagnetic Curie temperature and good compatibility in structure and conductivity with important III-V semiconductors, such as GaAs, etc.[21–23] Also half metallicity has been confirmed in superlattices $(CrAs)_1(MnAs)_1$ and $(CrAs)_2(MnAs)_2$ theoretically.[24]

One of the most important properties of DMSs is their Curie temperature. In fact, one DMS can be a potential candidate of spintronics only if its Curie temperature is higher than room temperature. The Curie temperature of some half-metallic Heusler alloys and pnictides have been systematically investigated by Bruno *et al.* within the mean-field approximation (MFA) and the random-phase approximation (RPA).[25–29] Especially, ZB CrAs is found to show Curie temperature above 1000 K. We deduce that by partly substituting Al for TMs in AlAs, some new ferromagnetic semiconductors, even HMFs, could be found, which might have a high Curie temperature too. So it is highly desirable to explore systematically ferromagnetic semiconducting alloys based on

AlAs. However, there is little work about this kind of materials.[30]

In this paper, a full-potential linear augmented plane waves plus local orbitals (FLAPW+lo) method has been used to investigate the structural stability, electronic structure, and magnetic properties of ZB $Al_{1-x}Cr_xAs$ systematically, with x ranging from 0.125 to 0.875. In addition, MFA of the classical Heisenberg Hamiltonian is used to estimate the Curie temperature. Particular attention is paid on the relation between properties and the Cr composition. An approximately monotonic relation between properties and the Cr compositions in $Al_{1-x}Cr_xAs$ has been found. These findings are important in explore high-performance devices based on $Al_{1-x}Cr_xAs$ and to understand the ferromagnetism in the ferromagnetic semiconductors or DMSs in depth.

The rest of the paper is organized as follows. In Sec. II, we present our calculational details, while the main results about structural stabilities are described in Sec. III. Further details about the electronic structure and half-metallic ferromagnetism in $Al_{1-x}Cr_xAs$ have been demonstrated in Sec. IV, with effects of the spin-orbital (SO) interaction and orbital magnetic moments discussed in Sec. V. The exchange parameters and the Curie temperature are presented in Sec. VI At last, we give the summary in Sec. VII and acknowledgments.

II. COMPUTATIONAL DETAILS

For calculations other than the exchange parameters, we employ a FLAPW+lo method within density-functional theory[31] (DFT), as implemented in the WIEN2K code.[32] The generalized gradient approximation[33] (GGA) is taken for the exchange-correlation potential. For core and valence states, we take the full relativistic calculation and its scalar approximation, respectively. The radii of the muffin-tin spheres (R_{mt}) are chosen to be 1.7 Bohr for all atoms when optimizing the cell volume and internal parameters in order to make sure that muffin-tin spheres do not overlap for various structures. For the electronic structure calculation, we set R_{mt} to be approximately proportional to the corresponding ionic radii and as large as possible, provided the muffin-tin spheres do not overlap each other. A plane-wave cutoff of $R_{mt} \times K_{\max} = 8.0$ has been adopted throughout our calculation and the angular expansion is made up to ten spheric harmonic functions in the muffin tins. Self-consistent calculations are considered to be converged when the integrated charge difference per formula unit, $\int |\rho_n - \rho_{n-1}| d\vec{r}$, is less than 0.000 05, where $\rho_{n-1}(\vec{r})$ and $\rho_n(\vec{r})$ are the input and output charge densities and the force acted on each atom is smaller than 1 mRy/Bohr.

An effective Heisenberg Hamiltonian

$$H_{\text{eff}} = -\sum_{i \neq j} J_{ij} \vec{s}_i \cdot \vec{s}_j \tag{1}$$

of the classic spin is used to describe the interatomic exchange interactions. J_{ij} is an exchange parameter between two $3d$ sites (i,j), which can be extracted from the *ab initio* total-energy results.[34] In CrAs, the exchange interactions are characterized mainly by that of the nearest Cr atoms.[29] For all Cr concentrations, a $\sqrt{2} \times \sqrt{2} \times 1$ supercell of original ZB cell is used, except for the $x=0.125$ case, where a $\sqrt{2} \times \sqrt{2} \times 2$ supercell is adopted. A state-of-the-art plane wave plus the ultrasoft pseudopotential method,[35] based on DFT (Ref. 31) and GGA,[33] is adopted for all these supercells. The electronic wave functions (charge densities) are expanded in a plane-wave basis set up to an energy cutoff of 25 Ry (300 Ry). 18 special **k** points are used in the first Brillouin zone (BZ) for the BZ integrations.

The Curie temperature can be estimated by MFA, RPA,[25–29] or Monte Carlo[34] method, providing that the exchange parameters are known. According to the work of Şaşıoğlu *et al.*, MFA method could give simple but reasonable estimation of the Curie temperature. In the MFA method of classical Heisenberg Hamiltonian, the Curie temperature is given by

$$T_C^{\text{MFA}} = \frac{2}{3k_B} \sum_{j \neq 0} J_{0j}, \tag{2}$$

where J_{0j} is the exchange parameter.

III. STRUCTURE STABILITY OF THE ZINC-BLENDE PHASE OF $Al_{1-x}Cr_xAs$

In order to investigate the structural stability of $Al_{1-x}Cr_xAs$ systematically, we consider the whole range of x from 0 up to 1.0. The $x=0$ and $x=1$ cases correspond to semiconducting AlAs and pnictide HMF CrAs, respectively, which have been studied widely. AlAs crystallizes at the ZB phase with space group 216, which has four AlAs units in the cubic cell. Substituting one, two, or three Als in the cubic cell for Crs, three ferromagnetic (FM) alloys, $Al_{0.75}Cr_{0.25}As$ (with space group 215), $Al_{0.5}Cr_{0.5}As$ (with space group 111), or $Al_{0.25}Cr_{0.75}As$ (with space group 215), can be obtained. In order to model the 0.125 and 0.875 substitutional cases, a supercell along the (110) direction of the original cubic ZB cell is constructed first, which contains eight AlAs units. Substituting one or seven Al for Cr in this supercell, $Al_{0.875}Cr_{0.125}As$ and $Al_{0.125}Cr_{0.875}As$ can be obtained, both with space group 115. The supercell along the (100) direction of original ZB cell has also been considered, which, however, results in a much higher total energy. Figure 1 shows the structures of $Al_{0.875}Cr_{0.125}As$, $Al_{0.75}Cr_{0.25}As$, and $Al_{0.5}Cr_{0.5}As$ from top to bottom. $Al_{0.125}Cr_{0.875}As$ and $Al_{0.25}Cr_{0.75}As$ can be obtained by interchanging Cr and Al atoms in $Al_{0.875}Cr_{0.125}As$ and $Al_{0.75}Cr_{0.25}As$ in Fig. 1.

As is well known, ZB structure is the ground state of semiconductor AlAs. However, for pnictide CrAs, the NiAs phase is more stable than the ZB one.[21] In order to investigate the stability of the ZB phase relative to the NiAs one, NiAs structures with the same Cr composition as the ZB structures are constructed. Full optimization of cells including total energy over the cell volume, c/a, and internal parameters for all these ZB and NiAs structures, is performed. A (meta)stable energy is used to indicate the stability of the ZB phase

$$\Delta E_0 = E_{\text{ZB}} - E_{\text{NiAs}}, \tag{3}$$

where E_{ZB} and E_{NiAs} denote the total energy of the ZB and NiAs phases at their equilibrium lattice constants, respec-

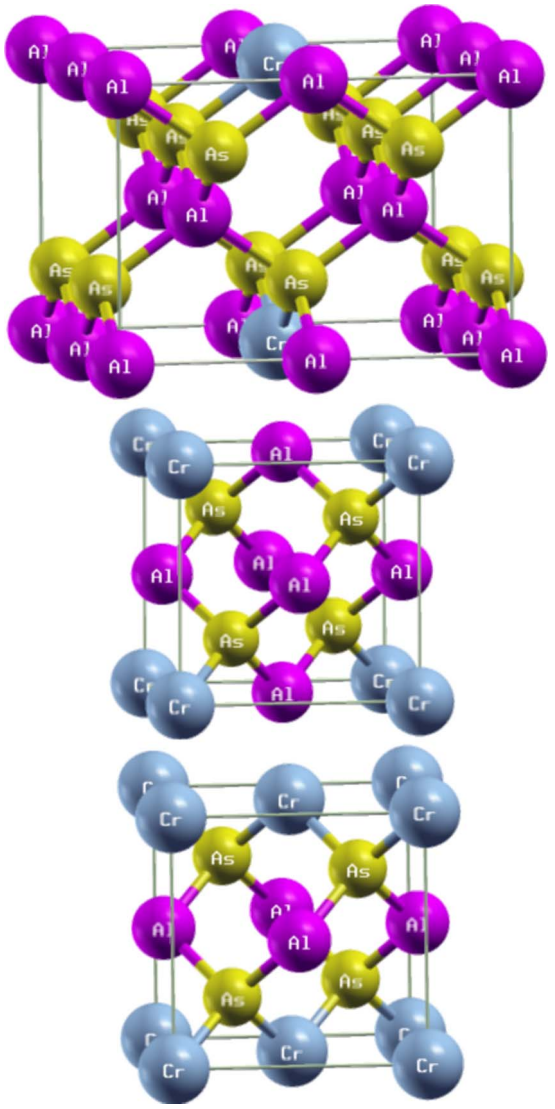

FIG. 1. (Color online) Structures of $Al_{1-x}Cr_xAs$, for x=0.125, 0.25, and 0.5 from top to bottom. Structures for x=0.875 and 0.75 cases can be obtained by interchanging Cr and Al atoms in top two figures.

tively. A positive value of ΔE_0 means that the ZB phase is less stable than the corresponding NiAs structure, whereas a negative ΔE_0 means a more stable ZB phase. ΔE_0 of $Al_{1-x}Cr_xAs$ for the whole range of x are listed in Table I. For CrAs, the calculated (meta)stable energy is as large as 0.84 eV, which is consistent with previous theoretical results.[21] It can be seen that there is a critical point for the Cr composition x, below which the ZB phase is more stable, whereas above which the NiAs phase is more stable. More precisely, the critical point can be shown by the heat of formation of both phases as follows:

$$E^H_{\mathrm{ZB(NiAs)}} = E_{\mathrm{ZB(NiAs)}} - xE^{\mathrm{CrAs}}_{\mathrm{NiAs}} - (1-x)E^{\mathrm{AlAs}}_{\mathrm{ZB}}, \qquad (4)$$

where $E^H_{\mathrm{ZB(NiAs)}}$ is heat of formation for the ZB or NiAs phase and $E^{\mathrm{CrAs}}_{\mathrm{NiAs}}$ and $E^{\mathrm{AlAs}}_{\mathrm{ZB}}$ are the total energies of CrAs and AlAs in their ground states. Figure 2 shows the calculated heat of formation per $Al_{1-x}Cr_xAs$ formula as a function of Cr composition x for both the ZB and NiAs phases. It can be seen that the ZB phase is more stable than the NiAs one when the Cr composition is less than 30%, where the ZB phase may exist as bulk samples or thick films. On the other hand, the ZB phase is less stable for larger x and can exist only as epitaxial films.

TABLE I. Presented are the equilibrium lattice constants (ELC, a for cubic cells, a/c for tetrahedral cells) per unit cell, (meta)stability energy (ΔE_0) of the ZB phase, and relative energy of the AFM structure with respect to the FM one (ΔE_1) of ZB $Al_{1-x}Cr_xAs$ with x range from 0 to 1.0. All energies are normalized with respect to the formula unit (Al, Cr)As.

Compounds	ELC (Å)	ΔE_0 (meV)	ΔE_1 (meV)
AlAs	5.73	−576	0
$Al_{0.875}Cr_{0.125}As$	8.11/5.71	−270	13
$Al_{0.75}Cr_{0.25}As$	5.72	−64	36
$Al_{0.5}Cr_{0.5}As$	5.69	304	4
$Al_{0.25}Cr_{0.75}As$	5.67	590	176
$Al_{0.125}Cr_{0.875}As$	7.99/5.63	690	221
CrAs	5.65	840	274

In order to investigate the relative stability of the FM phase with respect to the antiferromagnetic (AFM) one, various AFM structures for each FM ZB cell have been constructed and optimized. Relative stability of FM structure is indicated by the total-energy difference between the lowest AFM structure and the FM one as follows:

$$\Delta E_1 = E_{\mathrm{AFM}} - E_{\mathrm{FM}}, \qquad (5)$$

where E_{FM} and E_{AFM} are the total energies of the FM structure and the lowest AFM structure. A positive ΔE_1 means a more stable FM phase and a negative a less stable FM one. For all these FM and AFM structures, full optimization including total energy over cell volume, c/a, and internal parameters is performed. The results are summarized in Table I.

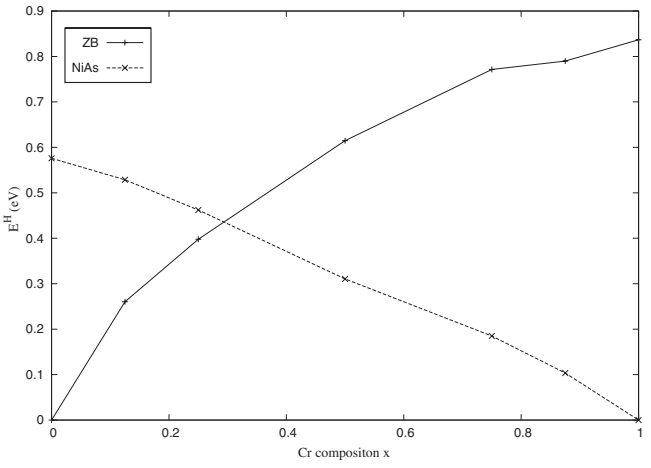

FIG. 2. Heat of formation for both the ZB and NiAs phases of $Al_{1-x}Cr_xAs$, where the solid line shows that of the ZB phase and the dashed line the NiAs one.

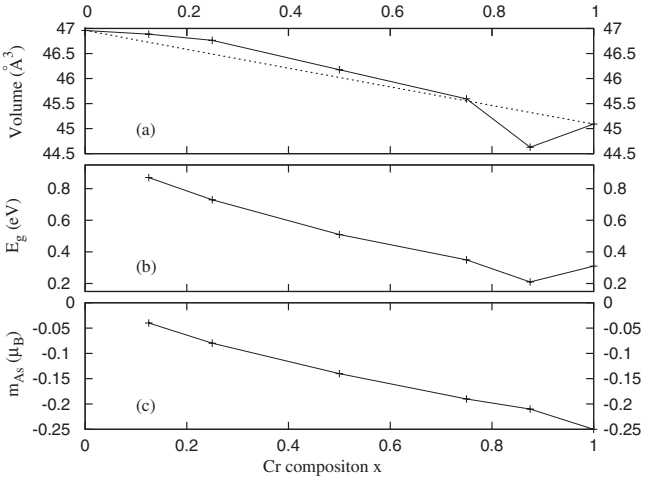

FIG. 3. The cell volume, the half-metallic gap, and the spin magnetic moment contributed by As atoms of $Al_{1-x}Cr_xAs$ as a function of the Cr composition x are shown in (a), (b), and (c) respectively.

We can see that the FM phase is more stable than the AFM one for all Cr compositions and the stability of the ferromagnetism is enhanced by the Cr composition except for $Al_{0.5}Cr_{0.5}As$.

In DMSs, equilibrium lattice constants and the concentration of impurities obey the Vegard's law, which states that[37–39]

$$a_{(III,\mathrm{TM})V}(x) = (1-x)a_{III-V} + xa_{\mathrm{TM}-V}, \tag{6}$$

where $a_{(III,\mathrm{TM})V}(x)$, a_{III-V}, and $a_{\mathrm{TM}-V}$ are lattice constants of $Al_{1-x}Cr_xAs$, AlAs, and CrAs. The calculated equilibrium lattice constants are listed in the second column of Table I. Figure 3(a) shows the cell volume of $Al_{1-x}Cr_xAs$ as a function of the Cr composition x. The dotted line represents the cell volume calculated by lattice constants according to the Vegard's law. We can see that except for the $x=0.875$ case, the calculated volumes obey the Vegard's law at large. For compounds with very high concentration of Cr, such as $Al_{0.125}Cr_{0.875}As$, there may be some other defects except for the standard substitutional Cr atoms, such as interstitial atoms, Al_{As} antisites, etc., which may cause the lattice constants and then the cell volumes to deviate from the Vegard's law.[38–40]

IV. ELECTRONIC STRUCTURE AND HALF-METALLIC FERROMAGNETISM

Presented in Fig. 4 are the spin-dependent total and partial densities of states (DOSs) for $Al_{1-x}Cr_xAs$ with x ranging from 0.125 to 0.875. The top of the valance band of AlAs is mainly attributed to As-4p states, hybridized with Al-(3s,3p), while the bottom of the conduction band is primarily attributed to Al-(4p,3d) and As-(4d,5s) states.[41,42] The calculated semiconducting gap of AlAs is about 1.5 eV, which is much smaller than the experimental value of 2.3 eV because of the well-known underestimation of DFT calculations. After introducing Cr atoms in AlAs, there are strong

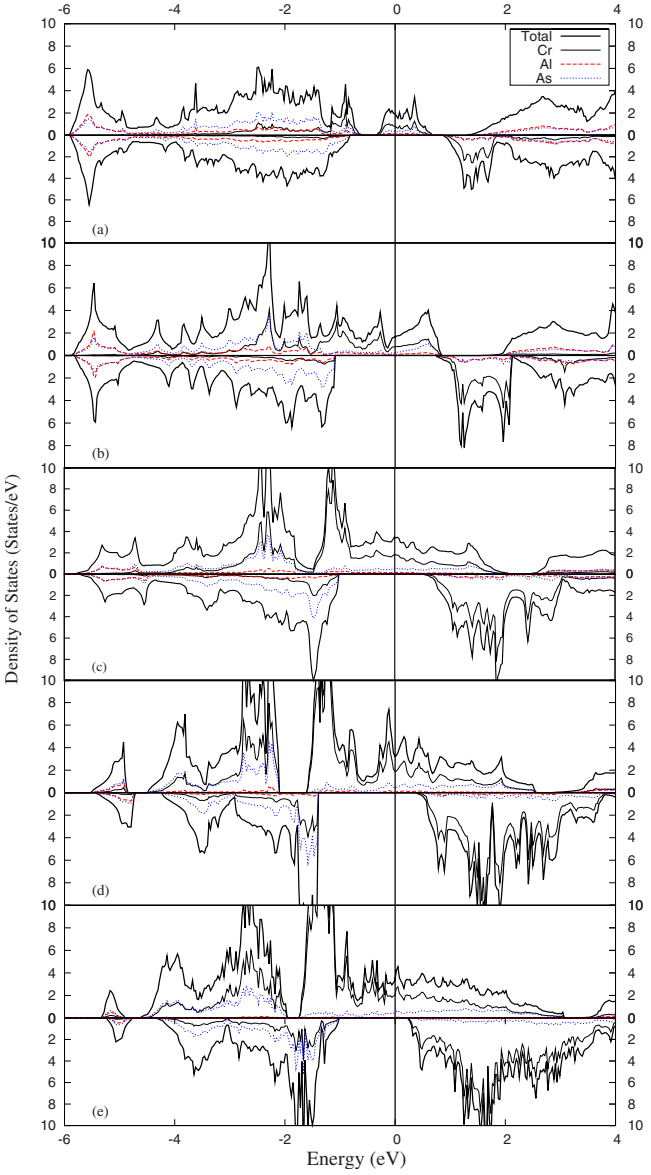

FIG. 4. (Color online) Spin-dependent DOSs of the ZB phase of $Al_{1-x}Cr_xAs$, for $x=0.125$, 0.25, 0.5, 0.75, and 0.875 are shown from (a) to (e), where the thick solid lines show the total DOSs, the thin solid lines the Cr partial DOSs, the dashed lines that of the Al, and the dotted lines that of the As.

hybridizations between Cr-3d and As-4p states, which will introduce some states in the majority-spin gap. Due to the exchange splitting of Cr-3d states, the minority-spin states of Cr-3d are pushed completely above the Fermi level, but keeping a minority-spin gap as in semiconducting AlAs, which is the origin of the half-metallic gap.

In order to analyze the bonding properties in detail, orbital projected DOS (PDOS) are needed. Because all these compounds have similar electronic structure, PDOS of $Al_{0.75}Cr_{0.25}As$ are taken as an example and shown in Fig. 5. As-4s states, which are mainly localized at nearly 11.0 eV below the Fermi level and bonding with Al-3s and -3p, are not shown in Fig. 5. The states at about −5.5 eV originate mainly from Al-3s states with a little hybridization with As-4p states. A slight splitting between the majority- and

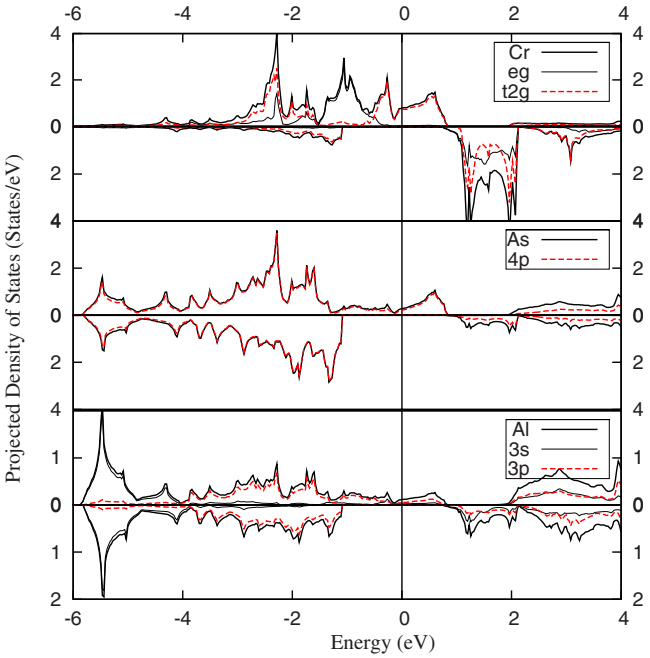

FIG. 5. (Color online) Presented from top to bottom are spin-dependent PDOSs of the ZB phase of $Al_{0.75}Cr_{0.25}As$. The top panel shows the Cr total DOS (the thick solid line), the Cr-*eg* PDOS (the thin solid line), and the Cr-*t*2*g* PDOS (the dashed line). The middle panel shows the As total DOS (the thick solid line) and the As-4*p* PDOS (the dashed line), while the last panel shows the Al total DOS (the thick solid line), the Al-3*s* PDOS (the thin solid line), and the Al-3*p* PDOS (the dashed line).

minority-spin states of the hybridized states of Al-3*s* and As-4*p* can be seen, which is due to the induction of the exchange splitting of Cr-3*d* states.

States near the Fermi level, which are mainly composed of Cr-3*d*, As-4*p*, and Al-3*s* and -3*p* states, are most important for the bonding properties and half-metallic ferromagnetism. Considering the majority-spin states at first, the states between −3 and −2 eV are mostly attributed to the strong Cr-*t*2*g*−As-4*p* hybridization and a relative weak hybridization between Cr-*t*2*g* and Al-3*p* states. They are the bonding states. The broad antibonding states begin at about −0.5 eV and also exhibit a mixed character of Cr-*t*2*g* with both As-4*p* and Al-3*p* states. The Cr-*eg* states are the nonbonding states and located in the bonding-antibonding gap. The minority-spin states exhibit a similar structure but shifted upward due to the strong exchange splitting of Cr-3*d* states. The bonding states which originate from the hybridization of Cr-*t*2*g* with As-4*p* and Al-3*p* states are located mainly between −2.0 and −1.4 eV below the Fermi level. Both the antibonding Cr-*t*2*g* states and the nonbonding Cr-*eg* states are pushed wholly above the Fermi level, keeping a minority-spin gap which is the origin of the half-metallic gap.

Combining Fig. 4 with Fig. 5, one can see that the spin splittings of Al-3*s* states increase with the Cr composition, which is consistent with the increase of the induced local magnetic moments of Al as shown in Table II. Although the bonding states and the nonbonding states change little with Cr compositions, the antibonding states broaden as the Cr composition increases. When the Cr compositions are very low, the antibonding states are localized in the majority-spin semiconducting gap with an extension of only about 0.7 eV. As *x* increases, however, the expansion of the antibonding states enhances, which could be as large as 3 eV in CrAs.

TABLE II. Presented are total magnetic moments per cell and magnetic moments localized on each site ($M_{Cr}/M_{Al}/M_{As}$) in unit of μ_B and half-metallic gap (E_g) in unit of eV of $Al_{1-x}Cr_xAs$ with *x* ranging from 0.125 to 1.0.

Compounds	m (μ_B)	$m_{Cr}/m_{Al}/m_{As}$ (μ_B)	E_g (eV)
$Al_{0.875}Cr_{0.125}As$	3.00	2.93/0.01/−0.04	0.87
$Al_{0.75}Cr_{0.25}As$	3.00	2.95/0.03/−0.08	0.73
$Al_{0.5}Cr_{0.5}As$	6.00	2.95/0.04/−0.13	0.51
$Al_{0.25}Cr_{0.75}As$	9.00	2.98/0.05/−0.19	0.35
$Al_{0.125}Cr_{0.875}As$	21.00	2.96/0.04/−0.22	0.23
CrAs	3.00	3.01/0/−0.25	0.31

An important property of HMFs is their half-metallic gap, defined as the minimum of E_{bc} and E_{tv}, where E_{bc} is the bottom energy of the minority-spin conduction bands with respect to the Fermi level and E_{tv} the absolute values of the top energy of the minority-spin valence bands also with respect to the Fermi level.[36] Half-metallic gaps of $Al_{1-x}Cr_xAs$ ($0.125 \leq x \leq 1.0$) are listed in the last column of Table II. It can be found that generally the half-metallic gaps become smaller with the increase of the Cr composition. The half-metallic gaps of $Al_{1-x}Cr_xAs$ as a function of the Cr composition *x* have been given in Fig. 3(b), where the half-metallic gaps vary in a similar manner as the cell volumes with respect to the Cr composition *x*. Therefore, the half-metallic gap could be tuned by the Cr composition in $Al_{1-x}Cr_xAs$. The exception occurs when *x* is equal to 0.875, which may be due to defects other than substitution and will be explained elsewhere. The total and local spin magnetic moments of $Al_{1-x}Cr_xAs$ have been listed in Table II. Each Cr atom contributes an integer total spin magnetic moment of exact $3\mu_B$, which is a notable character of HMFs. Figure 3(c) shows the local moments of As as a function of Cr composition, which is also similar to the Vegard's law.

V. EFFECTS OF THE SPIN-ORBITAL INTERACTION ON HALF-METALLIC FERROMAGNETISM

The half-metallicity can be suppressed by some factors, e.g., the SO interaction,[43] nonquasiparticle states,[44] defects,[45] surfaces, and interfaces, spin excitations at finite temperature, etc. The SO interaction exists even at $T \to 0$ and in the defect-free case for all elements. In this part, we concentrate mainly on effects of the SO interaction. The SO interaction can introduce a mixture of two spin channels, which cause some nonvanishing DOSs in the minority-spin band gap[43] and then the half metallicity is destroyed.

In order to demonstrate the influence of SO interaction on half metallicity in $Al_{1-x}Cr_xAs$ in detail, we have performed a fully GGA+SO calculation for all these compounds. The

TABLE III. Presented in the first four columns are orbital magnetic moments contributed by each Cr and As atom, the total orbital moments, and the total magnetic moments per cell including both spin and orbital contributions in unit of μ_B. Shown in the last column is the total energy difference between with and without the SO interaction per $Al_{1-x}Cr_xAs$ formula in unit of meV.

Compounds	m_{Cr}^{orb} (μ_B)	m_{As}^{orb} (μ_B)	m_{total}^{orb} (μ_B)	m_{total} (μ_B)	Δ_{SO} (meV)
$Al_{0.875}Cr_{0.125}As$	−0.0123	−0.0008	−0.0186	2.981	−8.8
$Al_{0.75}Cr_{0.25}As$	−0.0140	−0.0008	−0.0167	2.983	−9.9
$Al_{0.5}Cr_{0.5}As$	−0.0168	−0.0011	−0.0378	5.962	−12.4
$Al_{0.25}Cr_{0.75}As$	−0.0186	−0.0014	−0.0616	8.938	−12.9
$Al_{0.125}Cr_{0.875}As$	−0.0168	−0.0012	−0.1276	20.872	−13.5
CrAs	−0.0186	−0.0019	−0.0205	2.979	−14.3

strength of the SO interaction is manifested by the difference of total energy calculated with and without SO interaction, denoted by Δ_{SO}. In the last column of Table III, we give the calculated Δ_{SO} per $Al_{1-x}Cr_xAs$ formula. It can be seen that this total-energy difference increases with the Cr composition. Figure 6 presents the calculated DOSs of $Al_{1-x}Cr_xAs$ including the SO interaction, where the thick solid lines denote total DOSs, the thin solid lines the Cr-3*d* PDOSs, and the dashed lines the As-4*p* PDOSs. In order to manifest effects on the half metallicity, we focus on the energy range near the minority gap. The majority-spin DOSs are reflected into the minority-spin gaps for all these compounds due to the SO interaction. This reflection is relative small, giving a minority or majority DOS ratio of only 0.1% at the Fermi level and resulting a decrease of the spin polarization of only about 0.2% for all compounds. It is clear that considering the SO interaction, $Al_{1-x}Cr_xAs$ is not strictly half metallic anymore. However, because the SO interaction strength of these elements is relative low (no heavy elements) and the Fermi level is far away from the band edge,[46] all $Al_{1-x}Cr_xAs$ compounds remain a relative high spin polarization.

Another result of SO interaction is nonzero orbital magnetic moment. In Table III, we give the calculated localized orbital magnetic moments of Cr and As in the first two columns. The total orbital moments and total magnetic moments including both the spin and orbital contribution are listed in the third and fourth columns. One can see that the total magnetic moments become nonintegral for all $Al_{1-x}Cr_xAs$ if the SO interaction is considered, which is consistent with DOSs shown in Fig. 6. Particularly, the absolute value of the localized orbital moments of each atom increases with the Cr composition, except for the $x=0.875$ case which may also be related to some defects other than substitution.

VI. EXCHANGE PARAMETERS AND CURIE TEMPERATURE

Şaşıoğlu *et al.* did some systematic works about the magnetic exchange parameters and the Curie temperature of ZB pnictides by frozen-magnon approach and MFA (RPA),[29] where ZB CrAs is found to show a Curie temperature of above 1000 K. In ZB $Al_{1-x}Cr_xAs$, the nearest surrounding of a Cr atom is anionic As atoms. Other Cr atoms are located in

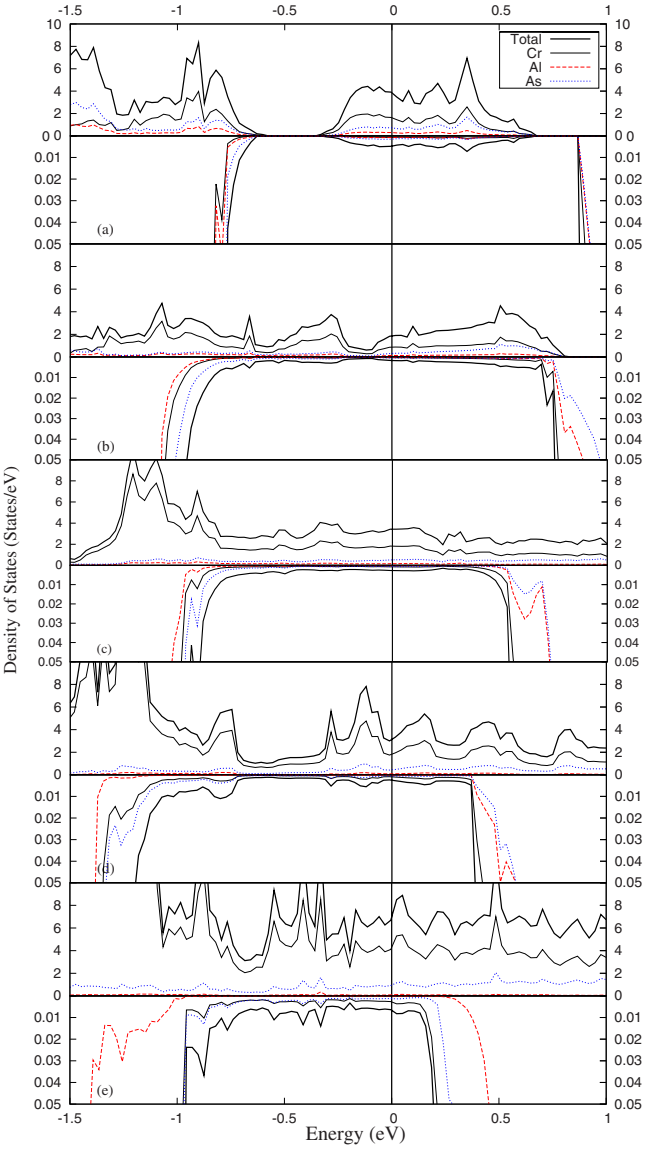

FIG. 6. (Color online) Spin-dependent DOSs, including the SO interaction, of the ZB phase of $Al_{1-x}Cr_xAs$ for x is equal to 0.125, 0.25, 0.5, 0.75, and 0.875 are shown from (a) to (e), where the thick solid lines show the total DOSs, the thin solid lines the Cr partial DOSs, the dashed lines that of the Al, and the dotted lines that of the As.

TABLE IV. Presented are the exchange parameters of nearest Cr atoms in unit of meV and the Curie temperatures given by MFA in unit of K for all $Al_{1-x}Cr_xAs$ compounds.

x	0.125	0.25	0.5	0.75	0.875	1.0
J_0	0.52	33.8	81.5	48.4	47.2	41.8
T_c^{MFA}	4	782	1259	1497	1825	1938

the next-nearest positions or further according to different Cr concentrations. Şaşıoğlu's work shows that the main exchange interaction in ZB CrAs is that between the TM atoms. Other interactions, such as that between TM-*sp*, *sp*-*sp* atoms, are small and can be neglected. In this work, only interaction of the nearest Cr sites is involved for all $Al_{1-x}Cr_xAs$ compounds.

Table IV lists the exchange parameters of the nearest Cr sites and the Curie temperature given by MFA for different Cr concentrations. One can see that the $x=0.5$ case has the largest exchange parameter. Different from the exchange parameters, the Curie temperature given by the MFA method (T_c^{MFA}) increases monotonically with the Cr concentrations. The exchange parameter and the Curie temperature of $Al_{0.875}Cr_{0.125}As$ are extremely small because of the relative large distance between two nearest Cr atoms. It can be seen that ZB $Al_{1-x}Cr_xAs$ with its Curie temperature above room temperature can be obtained by increasing the Cr concentrations.

VII. SUMMARY

In summary, we use an accurate full-potential density-functional method to study HMFs $Al_{1-x}Cr_xAs$ with x ranging from 0.125 to 0.875. It is found that there is a clear relation between the Cr composition and various properties. The equilibrium lattice constants follow the Vegard's law at large except for compounds with very high Cr composition, which may be due to defects other than substitutional atoms. More importantly, the half-metallic gaps follow a law similar to the Vegard's law as the equilibrium lattice constants. In order to explain this phenomenon, detailed analysis about the electronic structure has been performed. With increasing of the Cr composition, the antibonding states extended from 0.7 to 3 eV and the Fermi level moves upward. These two factors make the half-metallic gaps decrease.

The half metallicity could be destroyed by many factors. Strictly speaking, there is no perfect HMF because of the universal existence of the SO interaction. After considering the SO interaction, the strict half metallicity is destroyed for all $Al_{1-x}Cr_xAs$ compounds. The total-energy difference caused by the SO interaction and the spin-dependent DOSs are presented for all these compounds. The orbital moments and total magnetic moments including both the spin and orbital contribution have also been obtained. One of the most important properties of DMS is its critical temperature. By *ab initio* total-energy calculations for different magnetic configurations, exchange parameters of nearest Cr atoms and the Curie temperature by MFA for all compounds have been obtained. Except for the extremely low Cr concentration case, the Curie temperature is higher than the room temperature and increases with the Cr concentration. Our calculated results can be useful for a thorough understanding of magnetism in DMSs which might be promising candidates for future spintronic applications.

ACKNOWLEDGMENTS

This work is supported by the financial support from Sichuan Normal University (Project No. 08KYL08) and National Natural Science Foundation of China (Project No. 10747007).

*yhzhao.cd@gmail.com

[1] S. A. Wolf, D. D. Awschalom, R. A. Buhrman, J. M. Daughton, S. von Molnár, M. L. Roukes, A. Y. Chtchelkanova, and D. M. Treger, Science **294**, 1488 (2001); D. D. Awschalom and J. M. Kikkawa, Phys. Today **52**(6), 33 (1999).

[2] R. A. de Groot, F. M. Mueller, P. G. van Engen, and K. H. J. Buschow, Phys. Rev. Lett. **50**, 2024 (1983).

[3] W. E. Pickett and J. S. Moodera, Phys. Today **54**(5), 39 (2001).

[4] I. Galanakis, P. H. Dederichs, and N. Papanikolaou, Phys. Rev. B **66**, 134428 (2002).

[5] J. H. Park, E. Vescovo, H. J. Kim, C. Kwon, R. Ramesh, and T. Venkatesan, Nature (London) **392**, 794 (1998).

[6] J. S. Parker, S. M. Watts, P. G. Ivanov, and P. Xiong, Phys. Rev. Lett. **88**, 196601 (2002).

[7] H. Ohno, Science **281**, 951 (1998); T. Dietl, H. Ohno, F. Matsukura, J. Cibert, and D. Ferrand, *ibid.* **287**, 1019 (2000).

[8] S. Sanvito, G. Theurich, and N. A. Hill, J. Supercond. **15**, 85 (2002).

[9] S. J. Pearton, C. R. Abernathy, M. E. Overberg, G. T. Thaler, D. P. Norton, Y. D. Park, F. Ren, J. Kim, and L. A. Boatner, J. Appl. Phys. **93**, 1 (2003).

[10] H. Ohno, H. Munekata, T. Penney, S. von Molnar, and L. L. Chang, Phys. Rev. Lett. **68**, 2664 (1992); S. Sanvito, P. Ordejón, and N. A. Hill, Phys. Rev. B **63**, 165206 (2001).

[11] H. X. Liu, S. Y. Wu, R. K. Singh, L. Gu, N. R. Dilley, L. Montes, and M. B. Simmonds, Appl. Phys. Lett. **85**, 4076 (2004); S. Y. Wu and N. Newman, *ibid.* **89**, 142105 (2006); L. F. Zhu and B. G. Liu, J. Phys. D **41**, 215005 (2008).

[12] D. Kumar, J. Antifakos, M. G. Blamire, and Z. H. Barber, Appl. Phys. Lett. **84**, 5004 (2004); L. J. Shi, L. F. Zhu, Y. H. Zhao,

and B. G. Liu, Phys. Rev. B **78**, 195206 (2008).
[13] Y. H. Zhao, W. H. Xie, L. F. Zhu, and B. G. Liu, J. Phys.: Condens. Matter **18**, 10259 (2006); Y. H. Zhao and B. G. Liu, *ibid.* **20**, 135225 (2008).
[14] B. Monemar, Phys. Rev. B **8**, 5711 (1973).
[15] X. Zhu and S. G. Louie, Phys. Rev. B **43**, 14142 (1991).
[16] *Physics of Group IV Elements and III-V Compounds*, edited by O. Madelung, M. Schultz, and H. Weiss, Landolt-Börnstein, Numerical Data and Functional Relationships in Science and Technology, New Series, Group III, Vol. 17a (Springer, New York, 1982).
[17] C. M. Herzinger, P. G. Snyder, F. G. Celii, Y. C. Kao, D. Chow, B. Johs, and J. A. Woollam, J. Appl. Phys. **79**, 2663 (1996).
[18] H. Akinaga, T. Manago, and M. Shirai, Jpn. J. Appl. Phys., Part 1 **39**, L1118 (2000).
[19] J. F. Bi, J. H. Zhao, J. J. Deng, Y. H. Zheng, S. S. Li, X. G. Wu, and Q. J. Jia, Appl. Phys. Lett. **88**, 142509 (2006).
[20] V. H. Etgens, P. C. de Camargo, M. Eddrief, R. Mattana, J. M. George, and Y. Garreau, Phys. Rev. Lett. **92**, 167205 (2004).
[21] W. H. Xie, Y. Q. Xu, B. G. Liu, and D. G. Pettifor, Phys. Rev. Lett. **91**, 037204 (2003).
[22] L. J. Shi and B. G. Liu, J. Phys.: Condens. Matter **17**, 1209 (2005).
[23] A. A. Araújo, B. Laks, and P. C. de Camargo, Phys. Rev. B **74**, 172411 (2006).
[24] C. Y. Fong, M. C. Qian, J. E. Pask, L. H. Yang, and S. Dag, Appl. Phys. Lett. **84**, 239 (2004).
[25] L. M. Sandratskii and P. Bruno, Phys. Rev. B **67**, 214402 (2003).
[26] E. Şaşıoğlu, L. M. Sandratskii, and P. Bruno, Phys. Rev. B **70**, 024427 (2004).
[27] E. Şaşıoğlu, L. M. Sandratskii, P. Bruno, and I. Galanakis, Phys. Rev. B **72**, 184415 (2005).
[28] E. Şaşıoğlu, L. M. Sandratskii, and P. Bruno, J. Phys.: Condens. Matter **17**, 995 (2005).
[29] E. Şaşıoğlu, I. Galamakis, L. M. Sandratskii, and P. Bruno, J. Phys.: Condens. Matter **17**, 3915 (2005).
[30] B. Kang, W. Kim, Y. Song, and H. Kang, J. Magn. Magn. Mater. **310**, 2135 (2007).
[31] P. Hohenberg and W. Kohn, Phys. Rev. **136**, B864 (1964); W. Kohn and L. J. Sham, Phys. Rev. **140**, A1133 (1965).
[32] P. Blaha, K. Schwarz, P. Sorantin, and S. B. Trickey, Comput. Phys. Commun. **59**, 399 (1990).
[33] J. P. Perdew, K. Burke, and M. Ernzerhof, Phys. Rev. Lett. **77**, 3865 (1996).
[34] J. T. Wang, D. S. Wang, and Y. Kawazoe, Appl. Phys. Lett. **79**, 1507 (2001).
[35] S. Baroni, A. Dal Corso, S. de Gironcoli, and P. Giannozzi, 2001, http://www.pwscf.org
[36] W. H. Xie, B. G. Liu, and D. G. Pettifor, Phys. Rev. B **68**, 134407 (2003).
[37] A. R. Denton and N. W. Ashcroft, Phys. Rev. A **43**, 3161 (1991).
[38] J. Mašek, J. Kudrnovský, and F. Máca, Phys. Rev. B **67**, 153203 (2003).
[39] C. Caetano, L. G. Ferreira, M. Marques, and L. K. Teles, arXiv:0902.4368 (unpublished).
[40] I. Galanakis, K. Özdoğan, E. Şaşıoğlu, and B. Aktaş, Phys. Rev. B **74**, 140408(R) (2006).
[41] B. K. Agrawal and S. Agrawal, Phys. Rev. B **45**, 8321 (1992).
[42] H. Jin, G. L. Zhao, and D. Bagayoko, Phys. Rev. B **73**, 245214 (2006).
[43] Ph. Mavropoulos, K. Sato, R. Zeller, P. H. Dederichs, V. Popescu, and H. Ebert, Phys. Rev. B **69**, 054424 (2004).
[44] L. Chioncel, M. I. Katsnelson, R. A. de Groot, and A. I. Lichtenstein, Phys. Rev. B **68**, 144425 (2003).
[45] H. Ebert and G. Schütz, J. Appl. Phys. **69**, 4627 (1991).
[46] Ph. Mavropoulos and I. Galanakis, J. Phys.: Condens. Matter **19**, 315221 (2007).